

Multiscale modeling of effective elastic properties of fluid-filled porous materials

Mingchao Liu , Jian Wu , Yixiang Gan , Dorian AH Hanaor ,
C.Q. Chen

PII: S0020-7683(18)30482-7
DOI: <https://doi.org/10.1016/j.ijsolstr.2018.11.028>
Reference: SAS 10192



To appear in: *International Journal of Solids and Structures*

Received date: 20 November 2017
Revised date: 13 September 2018

Please cite this article as: Mingchao Liu , Jian Wu , Yixiang Gan , Dorian AH Hanaor , C.Q. Chen , Multiscale modeling of effective elastic properties of fluid-filled porous materials, *International Journal of Solids and Structures* (2018), doi: <https://doi.org/10.1016/j.ijsolstr.2018.11.028>

This is a PDF file of an unedited manuscript that has been accepted for publication. As a service to our customers we are providing this early version of the manuscript. The manuscript will undergo copyediting, typesetting, and review of the resulting proof before it is published in its final form. Please note that during the production process errors may be discovered which could affect the content, and all legal disclaimers that apply to the journal pertain.

Highlights

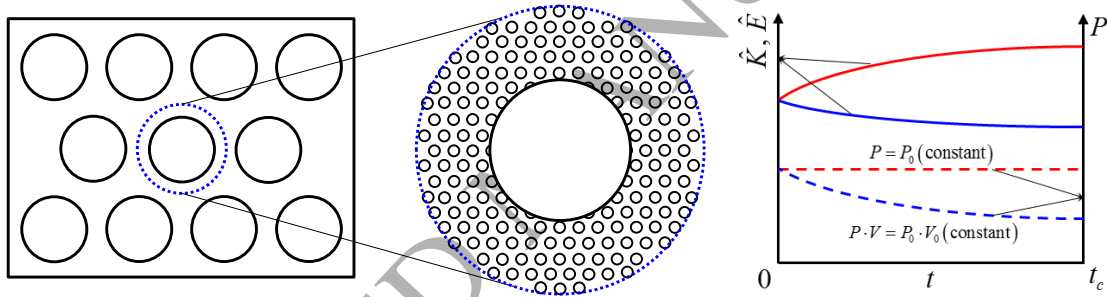
- A multiscale micromechanical homogenization framework is proposed for fluid-filled porous materials.
- The overall elastic properties of the fluid-filled porous materials are determined in the framework.
- The effects of pore distribution and fluid pressure on the effective elastic properties are quantified.
- By considering the fluid diffusion from macro- to micro-scale pores, evolution of the effective properties is predicted.

Multiscale modeling of effective elastic properties of fluid-filled porous materials

Mingchao Liu^{1,2}, Jian Wu¹, Yixiang Gan^{2,*}, Dorian AH Hanaor³, C.Q. Chen^{1,*}

1. *Department of Engineering Mechanics, CNMM & AML, Tsinghua University, Beijing 100084, China*
2. *School of Civil Engineering, The University of Sydney, Sydney, NSW 2006, Australia*
3. *Institute for Materials Science and Technology, Technische Universität Berlin, Berlin 10623, Germany*

Graphic abstract



*Corresponding authors.

Email addresses: chencq@tsinghua.edu.cn (C.Q. Chen), yixiang.gan@sydney.edu.au (Y. Gan).

Abstract

Fluid-filled porous materials are widely encountered in natural and artificial systems. A comprehensive understanding of the elastic behavior of such materials and its dependence on fluid diffusion is therefore of fundamental importance. In this work, a multiscale framework is developed to model the overall elastic response of fluid-filled porous materials. By utilizing a two-dimensional micromechanical model with porosity at two scales, the effects of fluid diffusion and the geometric arrangement of pores on the evolution of effective properties in fluid-filled porous materials are investigated. Initially, for a single-porosity model the effective elastic properties of the dry and fluid-filled porous materials with ordered pores are obtained theoretically by considering a geometrical factor, which is related to the distribution of pores in the matrix. Model predictions are validated by finite element simulations. By employing a double-porosity model, fluid diffusion from macro- to micro-scale pores driven by a pressure gradient is investigated, and the resulting time-dependent effective elastic properties are obtained for both constant pressure and constant injection rate conditions. It is found that the presence and diffusion of pressurized pore fluid significantly affect the elastic response of porous materials, and this must be considered when modeling such materials. It is expected that the proposed theoretical model will advance the understanding of the fluid-governed elastic response of porous materials with implications towards the analysis of geophysical, biological and artificial fluid-filled porous systems.

Keywords

Porous materials; Effective elastic properties; Micromechanical model; Double-porosity; Fluid diffusion

1 Introduction

As a type of heterogeneous materials, porous materials are usually composed of two components, a solid skeleton and pores. Pores may be either empty or filled with fluid (i.e., gas or liquid) (Gibson and Ashby, 1999; Gibson et al., 2010). The latter type is classified as fluid-filled porous materials, which are widely available in not only natural geophysical and biological systems, e.g., rock, plant, and bone, but also synthetic structures, such as hydrogels, tofu, and fluidic origami (Kim and Guyer, 2014). Predicting the effective elastic responses of fluid-filled porous materials is a challenging problem, which has attracted considerable attention in recent years, driven by its importance in diverse contexts such as estimating the stored amount of carbon dioxide (CO_2) during the injection in underground saline aquifer (Streit and Hillis, 2004; Leung et al., 2014; Szulczewski et al., 2014), predicting the time-dependent response of hydraulic actuators (Guiducci et al., 2014; Yuk et al., 2017), and designing fluid-filled acoustic metamaterials (Spadoni et al., 2014; Dorodnitsyn and Van Damme, 2016).

The particularity of this kind of materials is the strong coupling between the fluid pressure in the pores and the elastic deformation of the solid skeleton. This coupling induces a complex problem, as the overall elastic responses of fluid-filled porous materials are governed by the fluid pressure in the pores (Shafiro and Kachanov, 1997; Warner et al., 2000; Ayyagari and Vural, 2016). To describe the coupling of pore pressure, solid deformation, and macroscale stresses, in fluid saturated porous media, linear poroelasticity was established by Biot (1941) through a phenomenological approach. The thermodynamic background of this theory has since been confirmed by the mixture theory (Coussy et al., 1998) and the homogenization method (Thompson and Willis, 1991), as well as by the micromechanical approach (Cheng, 1997). More recently, Biot's constitutive relations for a linearly poroelastic material were also extended to cover the cases on finite deformation (Brown et al., 2014). Furthermore,

if the solid skeleton is not a continuum, i.e., there are some micro-scale pores in the solid matrix with a significantly smaller size than the macro-scale pores, the fluid in macro-scale pores will diffuse into the matrix (i.e., the small pores) driven by the pressure gradient between the two pore scales, resulting in the evolution of effective properties (Berryman and Wang, 1995; Rohan et al., 2012; Song et al., 2016). The evolving effective properties of fluid-filled porous materials are of importance to many practical applications and deserve further investigation towards a systematic understanding.

There has been a series of efforts made to understand the overall elastic responses of porous materials. As a simple case, the elastic constants and their porosity dependence in dry porous materials, i.e., pores are empty or filled with air, have attracted much attention (Mackenzie, 1950; Walsh et al., 1965; Wang, 1984; Day et al., 1992; Hu et al., 2000; Pabst et al., 2006; Li et al., 2010; Chen et al., 2015; Chen et al., 2017). However, the role of the spatial distribution of pores has rarely been considered. Goussev et al. (2000) showed that the transverse Poisson's ratio of porous materials depends strongly upon the spatial arrangement of the pores. More recently, Liu et al. (2016 (a) and (c)) also identified the effect of pore distribution on the elastic responses of ordered porous materials to inner pressure.

Naturally occurring porous materials, such as rocks and plants, generally contain fluid-filled pores, and effects of pressure on their overall elastic properties cannot be ignored (Brown and Korrington, 1975; Christensen and Wang, 1985; Georget et al., 2003; Gibson et al., 2010). More recently, synthetic porous materials have been designed by incorporating pressurized fluid in pores for use as tunable systems (Guiducci et al., 2014; Lv et al., 2014; Yuk et al., 2017). Although intrinsically phenomenological, substantial work on the theoretical modeling of effective responses in fluid-filled porous materials can be found in the literature (Shafiro and Kachanov, 1997; Warner et al., 2000; Kitazono et al., 2003; Vincent et al., 2009; Ma

et al., 2014; Guo et al., 2015; Su et al., 2017). Different methods for the prediction of overall mechanical properties of fluid-filled porous materials have been proposed by considering pressurized fluid as a compressible inclusion. For the poroelasticity, by introducing the Biot modulus as a parameter, the effect of fluid pressure on the effective response can be considered. However, as a phenomenological theory, the effect of the geometric distribution of pores is not captured by the Biot theory.

It must be noted that, in the various previous studies, the solid skeleton was assumed as a continuous phase with its interaction with pore fluid occurring only at the pore wall, assumed to be impermeable. However, many porous materials, such as rocks and bones, exhibit multiscale pore structures (Cowin, 2001; Tsakiroglou et al., 2009; Borgomano et al., 2017). In such materials, the structure can be considered as two or more interacting pore systems, which collectively have a strong influence on fluid transfer and effective elastic properties. The transport of fluid in such multiscale porous materials, especially the double-scale cases has been the subject of numerous studies (Moutsopoulos et al., 2001; Ba et al., 2008; Choo et al., 2016). Homogenization technologies have been proposed to explore the elastic behaviors of multi- (or double) scale porous materials (Auriault and Boutin, 1992, 1993; Boutin and Roye, 2015; Rohan et al., 2016). However, to date, few attempts have been made to incorporate the diffusion effect into homogenization techniques, and to further address the evolution of effective properties induced by fluid diffusion in the skeleton of porous materials.

In this paper, a two-dimensional (2D) micromechanical model, which consists of pores at two scales, is employed to develop a multiscale framework to analyze the overall elastic responses of the fluid-filled porous materials. This model allows for the coupling of fluid pressure and the deformation of the solid matrix at each pore scale and for fluid diffusion from macro-scale to micro-scale pores imbedded in a non-continuum skeleton driven by a pressure gradient. Based on this micromechanical

model, a theoretical model is proposed to predict the effective elastic properties of porous materials with/without pressurized pore fluid and is validated by finite element method (FEM) simulations. With this model, time-dependent elastic properties are obtained for constant and variable fluid pressure cases.

2 A micromechanical model of porous materials with double porosity

In order to investigate the overall elastic properties of fluid-filled porous materials, a 2D micromechanical model with double-porosity is considered. As shown in Fig. 1, a porous material is represented by double-scale periodically distributed pores imbedded in an elastic solid. At the macro-scale, see Fig. 1(a), the cylindrical pores are arranged in a well ordered 2D triangular lattice, and all pores are filled with pressurized fluid. A unit cell comprising a thick-wall cylinder from the macro-scale porous structure is shown in Fig. 1(b), and micro-scale cylindrical pores are distributed in the cylinder wall. The micro-scale pore structure within the solid skeleton is shown in Fig. 1(c), with a similar triangular distribution.

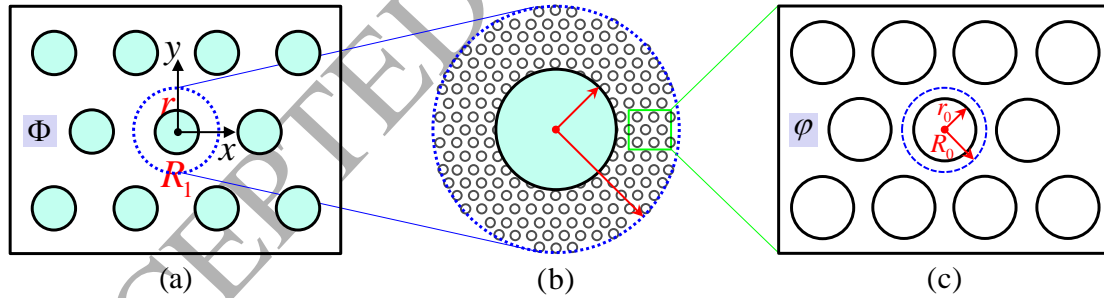


Fig. 1. Schematic representation of a porous material with double porosity: (a) Macro-scale pores filled with pressurized fluid; (b) a unit cell containing pores at two scales; (c) the solid skeleton containing micro-scale pores. Only the triangular distribution of pores is shown as an example.

It should be noted that the considered macro-scale pores are much larger than the micro-scale pores and much smaller than the dimensions of the overall structure. Accordingly, the porous material can be treated as a continuum solid in representing its overall mechanical behavior. Moreover, we assume the presence of fine diffusion

pathways within the solid matrix, facilitating the transport of fluid from macro- to micro-scale pores. Additionally, fluid flow between pores at the same scale is assumed to be restricted. For simplicity, the pores within each level are assumed with the same size.

3 Effective elastic properties of fluid-filled porous materials

Fluid pressure acting on pore walls can have a significant effect on the homogenized mechanical behavior of porous materials. In this section, we examine the overall elastic responses of fluid-filled porous materials based on the single-scale micromechanical model as described in Section 2.

3.1 Elastic properties of dry porous materials

We first consider a dry porous material, in which the pores are empty or filled with air. Under ambient conditions, the effects of air pressure on the deformation of the solid skeleton are negligible. The effective bulk modulus can be obtained by analyzing the deformation of porous samples under equi-biaxial external load, as shown in Fig. 2(a). It is not easy to directly solve the stress and deformation fields of this structure, on account of the interaction of microstructures (i.e., the ordered pores arranged in the matrix). However, Gor et al. (2015) pointed out that the overall deformation of a plate with many pores can be approximately represented by the deformation of a unit cell comprising a homogeneous cylinder. Our previous works (i.e., Liu et al. 2016 (a) and (c)) further showed that each unit cell is affected by its neighboring cylinders, implying that the outer boundary conditions of the cylinder are related to the geometrical arrangement of the pores. This single-pore model will be extended here to calculate the bulk modulus of the dry porous material.

In order to calculate the bulk modulus of porous materials through the single-pore model, the inner and outer boundaries have to be determined. The deformation of the

porous sample subjected to equi-biaxial external tension, σ_o in Fig. 2(a), can be considered as a combination of two components: I. Uniform deformation as shown in Fig. 2(b), i.e., the same uniform loads are applied on the outer boundary of the sample and the pore surfaces; II. Pore-load deformation, as shown in Fig. 2(c), i.e., the internal pressure is only applied on the pore surface, and the outer boundary of the sample is free. For the uniform deformation case, the outer boundary of the unit cylinder can be obtained as $p_1 = \sigma_o$. For the pore-load deformation case, Liu et al. (2016 (a) and (c)) gave the outer boundary condition as $p_{II} = \alpha \xi_i \sigma_o$, where α is a geometrical factor related to the interaction of neighboring pores and depending on the arrangement of pores, i.e., $\alpha = 1/3$ for porous materials with a triangular lattice. For materials with a square lattice pore arrangement, considering the symmetry of both the structure and the loading conditions, the applicability of the single-pore model is also valid, with $\alpha = 1/2$. Here, $\xi_i = r_i^2 / R_i^2$ (r_i and R_i are the inner and outer radii of the cylinder unit cell, respectively) is a dimensionless porosity factor related to the porosity φ_i of the porous material by $\xi_i = (2\sqrt{3}/\pi) \cdot \varphi_i$ for triangular lattice or $\xi_i = (4/\pi) \cdot \varphi_i$ for square lattice. Subscript $i = 0$ and 1 refer to the micro- and macro-scale pores, respectively.

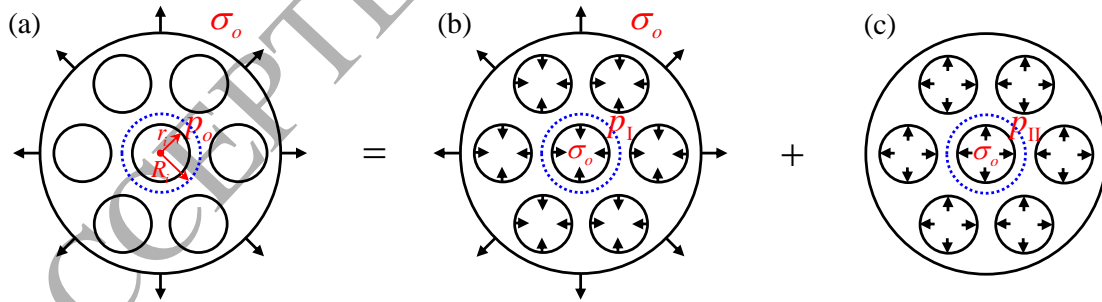


Fig. 2. Schematics of the superposition method used to determine the bulk modulus of porous materials: (a) a porous sample subjected to external equi-biaxial tension, which can be superposed by (b) a porous sample subjected to external equi-biaxial tension and the uniform pore pressure, and (c) a porous sample subjected to uniform pore pressure. The blue dotted lines represent the outer boundaries of the cylindrical unit cell.

By superposing the two components, the outer boundary condition of the unit cylinder

in Fig. 2(a) can be obtained as $p_o = \sigma_o (1 - \alpha \xi_i)$. In the case of plane stress, the radial displacement of the thick-wall cylindrical unit cell can be calculated according to the classical theory of elasticity (Timoshenko and Goodier, 1970)

$$u_r(r) = \frac{1}{E_i} \left[(1 - \nu_i) \frac{R_i^2 p_o}{R_i^2 - r_i^2} r + (1 + \nu_i) \frac{R_i^2 r_i^2 p_o}{R_i^2 - r_i^2} \frac{1}{r} \right], \quad (1)$$

where E_i and ν_i are Young's modulus and Poisson's ratio of the solid matrix, respectively. The volumetric strain of the cylinder unit cell is

$$\theta = \frac{u_r(R_i) \cdot 2\pi R_i}{\pi R_i^2} = 2 \cdot \frac{u_r(R_i)}{R_i}. \quad (2)$$

Substituting Eq. (1) into Eq. (2), the effective bulk modulus of dry porous materials can be obtained by the definition $\bar{K} = \sigma_o / \theta$ as

$$\bar{K}_i = \frac{E_i}{2} \cdot \frac{(1 - \xi_i)}{\left[(1 - \nu_i) + (1 + \nu_i) \xi_i \right] (1 - \alpha \xi_i)}. \quad (3)$$

It can be found that the effective bulk modulus of dry porous materials (i.e., \bar{K}_i) depends on not only the mechanical properties (i.e., elastic modulus E_i and Poisson's ratio ν_i) of the solid matrix, but also the porosity φ_i in terms of ξ_i and the geometrical arrangement of pores through the factor α .

It is noted that the geometrical arrangement of pores can have a significant effect on the overall elastic deformation. In particular, the transverse Poisson's ratio of a system having triangularly packed pores increases with porosity while that of a square packed array decrease (Goussev et al., 2000). This porosity dependence of Poisson's ratio cannot be captured by existing theoretical models. To fill this gap, we present a semi-empirical equation by adopting the geometric factor α , introduced by Liu et al. (2016 (a) and (c)) to describe the effect of pore distribution on the pore-load modulus, to relate the effective Poisson's ratio to the porosity of the porous material as

$$\bar{v}_i = 1 - \left[(1 - v_i) + (1 + v_i) \xi_i \right] (1 - \xi_i)^2 \cdot \text{Exp} \left\{ \frac{3\alpha \xi_i [2 + (1 + \alpha) \xi_i]}{2 [2 - (2 - \alpha) \xi_i]} \right\} . \quad (4)$$

For an isotropic elastic material, there are only two independent elastic parameters. For a planar problem, the effective Young's modulus can be obtained through the relation of $1 - \bar{v}_i = \bar{E}_i / 2\bar{K}_i$ combining with Eqs. (3) and (4) as

$$\bar{E}_i = E_i \cdot \frac{(1 - \xi_i)^3}{1 - \alpha \xi_i} \cdot \text{Exp} \left\{ \frac{3\alpha \xi_i [2 + (1 + \alpha) \xi_i]}{2 [2 - (2 - \alpha) \xi_i]} \right\} . \quad (5)$$

By means of Eqs. (3)-(5), the elastic properties of a porous material can be related to the porosity and the arrangement of pores.

It should be mentioned that E_i and v_i are the intrinsic elastic constants of the solid matrix of the micro-scale porous structure (i.e., $i = 0$). However, for the macro-scale porous structure (i.e., $i = 1$), E_i and v_i should be the homogenized elastic constants of the non-continuum skeleton. Furthermore, it should also be noted that the stiffness of a porous material having a square lattice can be considered as isotropic only under extreme hypothetical conditions in which porosity is sufficiently low and the so-called macro-pores are distributed quite sparsely. However, from a more accurate perspective, the stiffness of materials with a square lattice pore arrangement is orthotropic, and two stiff and two compliant directions can be found (Gibson and Ashby, 1999). Due to the symmetrical pore distribution, the relation of $1 - \bar{v}_i = \bar{E}_i / 2\bar{K}_i$ is also valid for the definition of elastic constant at principal directions.

In order to validate the proposed theoretical model of the overall elastic properties, i.e., Eqs. (3)-(5), FEM simulations are performed to calculate to the effective elastic constants of porous materials with triangular and square lattices. A 2D FEM model of a porous plate with ordered pores is established, as illustrated in Fig. 1(c). The left and bottom surfaces are constrained in the x and y directions, respectively, while the right

and top surfaces are subjected to uniform tension. Numerical experiments show that a FEM model with 15×17 unit cells for porous sample with triangular (and 15×15 for square) lattice is sufficient to show the homogenized responses of the corresponding porous materials. Moreover, a mesh sensitivity study has been conducted to confirm the numerical convergence of FEM models. The constituent solid matrix is assumed to be linear elastic with Young's modulus $E_0 = 70 \text{ GPa}$ and Poisson's ratio $\nu_0 = 0.3$.

The FEM simulated porosity dependent effective elastic constants of the porous material are shown in Figs. 3(a)-(c) for the bulk modulus, Young's modulus and Poisson's ratio, respectively. For each case, pore distributions of triangular and square lattices are considered. The corresponding theoretical predictions given by Eqs. (3)-(5) with different geometrical arrangement factors are included as solid lines for the purpose of comparison. For all three cases, one can find that the proposed theoretical model agrees well with the FEM results with different pore distributions. In particular, the opposing relationships between the effective Poisson's ratio and porosity can be qualitatively predicted by employing the geometric factor. The theoretical model of Eqs. (3)-(5) will be used to the further analysis of the effects of fluid pressure and diffusion on the overall elastic properties of fluid-filled porous materials.

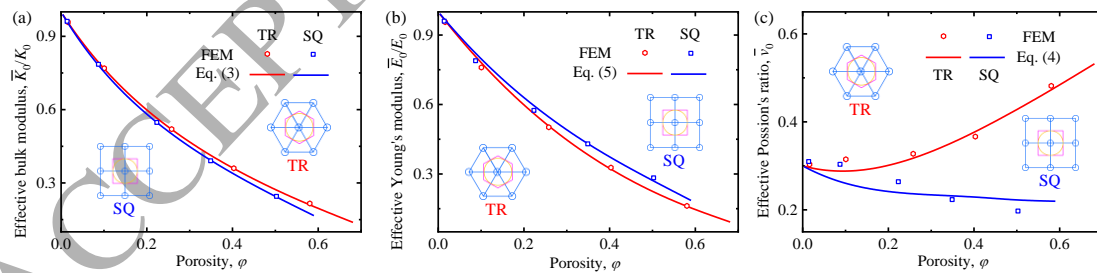


Fig. 3. Comparison of FEM simulations (symbols) and theoretical predictions (lines) of the effective elastic constants of porous materials with triangular (TR) and square (SQ) lattice as a function of porosity: (a) the normalized effective bulk modulus; (b) the normalized effective Young's modulus; (c) the effective Poisson's ratio.

3.2 Effect of fluid pressure

When pores are filled with pressurized fluid, the deformation of a solid skeleton can be significantly affected by the fluid pressure. Accordingly, the overall elastic properties of these materials depend upon fluid pressure (Warner et al., 2000; Gibson et al., 2010). Here we investigate the dependence of the effective properties of porous materials on the fluid pressure from a micromechanical point of view. The pressurized fluid within the pores is described by pressure boundary conditions on the wall of the pores imbedded in a solid matrix. For simplicity, the effect of pore deformation upon fluid pressure is neglected.

In order to determine the effective properties of the fluid-filled porous material, we consider a reference case of a porous material filled with pressurized fluid (a representative volume element is shown in Fig. 4(b)). Under external load, the porous material will deform, as shown in Fig. 4(c). Since the solid matrix is linearly elastic, the deformed state can be obtained by superimposing the pore pressure and external load on the dry porous material (i.e., the pressure free state, see Fig. 4(a)). As we have discussed in the preceding section, the effective elastic constants of dry porous materials, i.e., \bar{K}_i , $\bar{\nu}_i$ and \bar{E}_i , can be obtained from Eqs. (3)-(5). Here we are going to relate the effective elastic constants of fluid-filled porous materials (i.e., \tilde{K}_i , $\tilde{\nu}_i$ and \tilde{E}_i) to the fluid pressure, P_f .

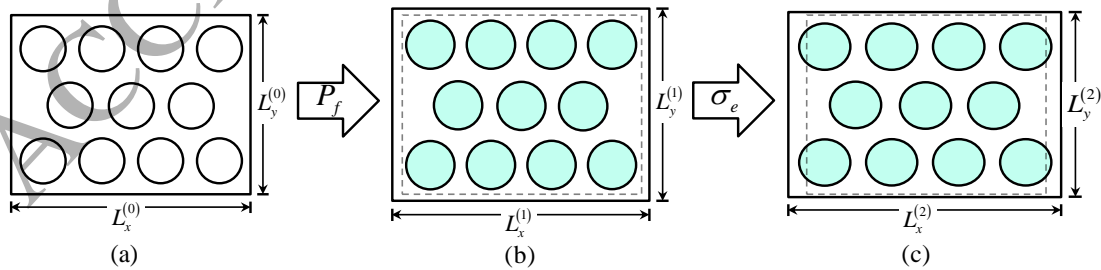


Fig. 4. Schematic representation of the deformation of a fluid-filled porous material subjected to inner fluid pressure and external load: (a) Porous structure with empty pores (pressure free); (b) The reference configuration of porous materials including pore pressure; (c) The deformed configuration of pressurized porous materials subjecting external load. $L_x^{(j)}$ and $L_y^{(j)}$ ($j = 0, 1$ and 2) refer to the dimensions of

the porous material under different states at x - and y -directions, respectively.

The deformation of the fluid-filled porous materials due to the external uniaxial tensile load, σ_e , can be obtained as

$$\sigma_e / \tilde{E}_i = L_x^{(2)} / L_x^{(1)} - 1, \quad (6)$$

where \tilde{E}_i is the effective Young's modulus of the fluid-filled porous materials. $L_x^{(1)}$ and $L_x^{(2)}$ are the x -direction dimensions of the undeformed and deformed fluid-filled porous materials and can also be given from the porous materials without fluid as

$$L_x^{(1)} = (P_f / M_i + 1) L_x^{(0)}, \quad (7)$$

$$L_x^{(2)} = (P_f / M_i + \sigma_e / \bar{E}_i + 1) L_x^{(0)}. \quad (8)$$

Here, $L_x^{(0)}$ is the x -direction dimension of the porous materials without fluid, P_f is the fluid pressure in the porous materials, and the pore-load modulus, M_i , is given by Liu et al. (2016 (a) and (c)) as

$$M_i = \frac{E_i (1 - \xi_i)}{(1 - \nu_i)(1 - \alpha)\xi_i - (1 + \nu_i)\xi_i(\alpha\xi_i - 1)}. \quad (9)$$

By substituting Eqs. (7) and (8) into Eq. (6), the effective Young's modulus can be obtained with an explicit form as

$$\tilde{E}_i / \bar{E}_i = 1 + P_f / M_i, \quad (10)$$

where \bar{E}_i and M_i are effective properties of the porous materials without fluid given by Eq. (5) and Eq. (9), respectively. It is seen that the effective Young's modulus of the fluid-filled porous material is linearly dependent on the pore pressure.

The effective bulk modulus can be obtained according to the similar analysis through the micromechanical model, and the corresponding expression is

$$\tilde{K}_i / \bar{K}_i = 1 + P_f / M_i, \quad (11)$$

where \bar{K}_i is the effective bulk modulus of the dry porous material given by Eq. (3). The linear dependence of the effective bulk modulus on the pore pressure is further evident. Considering the relation of $1 - \tilde{\nu}_i = \tilde{E}_i / 2\tilde{K}_i$, by combining Eqs. (10) and (11), the effective Poisson's ratio of the fluid-filled porous material can be found independent of the pore pressure, i.e., $\tilde{\nu}_i = \bar{\nu}_i$.

To verify the proposed theoretical model for effective moduli considering the effect of fluid pressure, FEM simulations are employed to calculate the effective elastic constants of fluid-filled porous materials with square lattice form. The FEM simulated pore pressure-dependent effective Young's modulus and bulk modulus of the porous material, normalized by the corresponding moduli of the solid matrix, are shown in Fig. 5(a) and (b) as symbols, respectively. Four different porosities (i.e., $\varphi = 0.26, 0.40, 0.58$ and 0.79) are considered for each case. The corresponding theoretical predictions given by Eqs. (10) and (11) are also included as lines for comparison. For both cases, one can find that the theoretical model can accurately predict the FEM results. It further confirms that the effective moduli of fluid-filled porous materials are indeed linearly dependent on the pore pressure, which is qualitatively consistent with the results of Gibson and Ashby (1999).

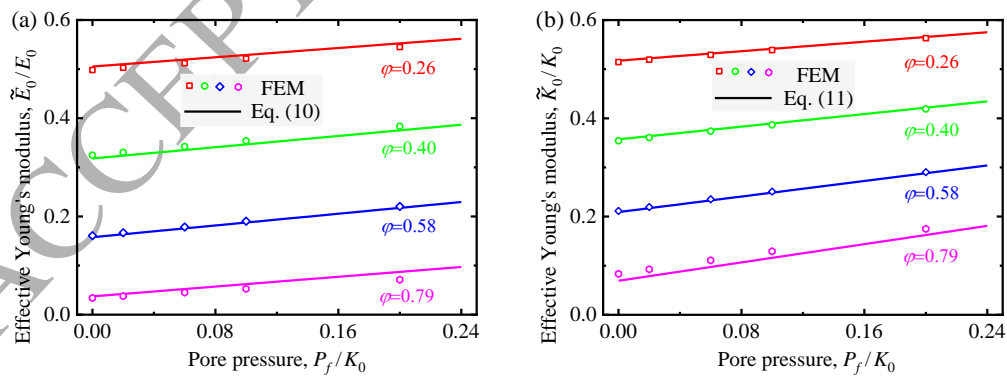


Fig. 5. Comparison of FEM simulations (symbols) and theoretical predictions (lines) of the effective elastic moduli of fluid-filled porous materials as a function of pore pressure: (a) the normalized effective Young's modulus; (b) the normalized effective bulk modulus.

4 Diffusion-induced evolution of effective properties

For fluid-filled porous materials having non-continuum matrixes, i.e., there are some micro-scale pores imbedded in the solid skeleton, the fluid in the macro-scale pores can diffuse into the solid skeleton driven by pressure gradient. The transfer and redistribution of pressurized fluid can also affect the overall elastic response. Here we investigate this diffusion-induced evolution through a micromechanical model with double- porosity, as illustrated in Fig. 1.

4.1 Fluid diffusion induced heterogeneity of porous material

Let us first consider the pressure-driven fluid diffusion from macro-scale pores to micro-scale pores. A thick-wall cylinder unit cell containing a macro-scale pore, which is filled with pressurized fluid, is shown in Fig. 6(a). It is assumed that the micro-scale pores at the diffused region are fully filled with the pressurized fluid (see Fig. 6(b)), and the pressure at these micro-scale pores is equal to the one at the macro-scale pore. The pressure-driven diffusion of fluid is similar to capillary-driven penetration in porous media, and can be described by Darcy's law (Whitaker, 1986). The fluid front r , i.e., the interface between fluid-filled micro-scale pores and empty ones, see the blue line in Fig. 6(a), moves from the inner boundary r_1 to the outer boundary R_1 of the cylinder unit cell during diffusion. The variation of the fluid front against diffusion time can be obtained as (Conrath et al., 2010; Liu et al., 2016 (b))

$$\left(\frac{r}{r_1}\right)^2 \left(\ln \frac{r}{r_1} - \frac{1}{2} \right) + \frac{1}{2} = \frac{t}{t_0}, \quad (12)$$

where $t_0 = \mu \varphi_0 r_1^2 / 2kP_f$ is a time scale, in which μ is the viscosity of the fluid, φ_0 the porosity of the solid skeleton with micro-scale pores, k the permeability of the porous skeleton, and P_f the pressure of the macro-scale pores. The fluid front position can be predicted quantitatively by Eq. (12).

It should be noted that here we consider the diffusion of fluid in the skeleton within micro-scale pores. The effect of the microstructure (e.g., the size and spatial distribution of the micro-pores) on the diffusion process can be reflected by homogenized macroscopic parameters, i.e., porosity and permeability. For example, a quantitative relation can be established to correlate the permeability and the distribution and size of micro-pores (Sobera and Kleijn, 2006).

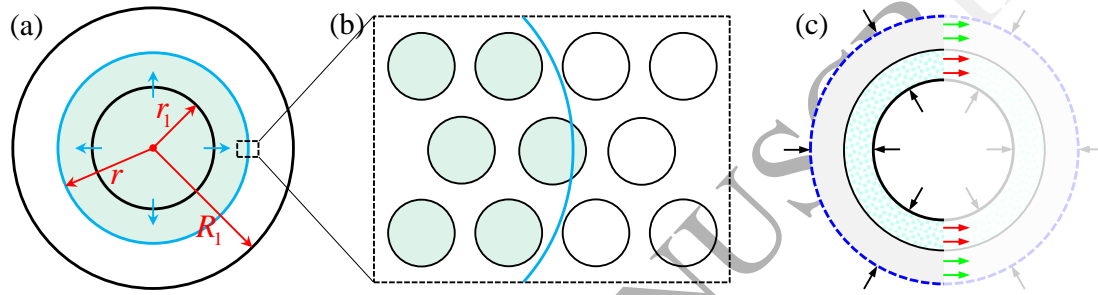


Fig. 6. Schematics of the pressure-driven fluid diffusion from macro-scale pores to micro-scale pores and its induced heterogeneity: (a) A cylindrical unit cell with pressurized fluid filled macro-scale pore; (b) The interface between fluid-filled micro-scale pores and empty ones; (c) The illustration of parallel model used to homogenize the porous material with partially pressurized micro-scale pores.

When fluid diffuses into micro-porous matrix from the macro-scale pores, the micro-scale pores behind the fluid front are filled by pressurized fluid, while those ahead of the fluid front remain empty, as shown in Fig. 6(b). For simplicity, we ignore the pressure gradient within the fluid-filled phase. As we have shown in Section 3.2, the effective elastic properties of the fluid-filled porous material are governed by pore pressure. Thus, the cylindrical unit cell becomes a heterogeneous structure consisting of two layers, see Fig. 6(a). For the dry outer layer, the effective properties (i.e., \bar{K}_0 , $\bar{\nu}_0$, \bar{E}_0 and \bar{M}_0) are obtained from Eqs. (3)-(5), and (9) by setting subscript $i = 0$. For the fluid-filled inner layer, the effective properties (i.e., \tilde{K}_0 , $\tilde{\nu}_0$ and \tilde{E}_0) can be obtained from Eqs. (10) and (11) with $i = 0$. These two layers form the new skeleton of the macro-scale porous structure which can be regarded as a composite structure with two phases (Wang et al., 2017). Under the inner and outer loads, as

shown in Fig. 6(c), the parallel model can be employed to homogenize this two-phase composite (Christensen, 2012). The homogeneous Young's modulus of this composite skeleton can be obtained as

$$E_1 = (1 - \phi) \cdot \bar{E}_0 + \phi \cdot \tilde{E}_0 \quad , \quad (13)$$

where \bar{E}_0 and \tilde{E}_0 are Young's moduli of the dry outer layer and fluid-filled inner layer, respectively, and ϕ is the volume fraction of the inner fluid-filled layer with

$$\phi = (r^2 - r_1^2) / (R_1^2 - r_1^2) \quad . \quad (14)$$

Here, r is the fluid front position, and r_1 and R_1 are the inner and outer radii of the cylindrical unit cell, respectively. It should be mentioned that the values of r_1 and R_1 are restricted by the porosity ϕ_1 in terms of ξ_1 , and cannot be completely arbitrary. In addition, the relation between ϕ_1 and ξ_1 is depending on the arrangement of the macropores. Similar to Eq. (13), the homogeneous bulk modulus can be expressed as

$$K_1 = (1 - \phi) \cdot \bar{K}_0 + \phi \cdot \tilde{K}_0 \quad , \quad (15)$$

where \bar{K}_0 and \tilde{K}_0 are bulk moduli of the dry and fluid-filled layers, respectively. As the effective Poisson's ratio of the fluid-filled layer is independent of fluid pressure, i.e., $\tilde{\nu}_0 = \bar{\nu}_0$, the homogeneous Poisson's ratio can also be obtained as $\nu_1 = \bar{\nu}_0$.

The effective elastic properties of the macro-scale dry porous structure containing partial filled micro-scale pores (see Section 3.1), i.e., \bar{K}_1 , $\bar{\nu}_1$, \bar{E}_1 and M_1 , can be obtained from Eqs. (3)-(5), (9) by setting subscript $i = 1$, with elastic constants of the homogeneous solid matrix obtained from Eqs. (13) and (15). It should be mentioned that the pore-load modulus of macro-scale dry porous structure M_1 can also be calculated through the theoretical model given by Liu et al. (2016 (c)). To unify, here we use the equivalent model of Eq. (9) combined with the homogeneous parameters. Similarly, as shown in Section 3.2, the effective properties of the macro-scale fluid-filled porous structure containing partially filled micro-scale pores (i.e., \tilde{K}_1 , $\tilde{\nu}_1$,

\tilde{E}_1) can be calculated through Eqs. (10) and (11) with a subscript $i = 1$.

To validate the double-scale approach, the effective moduli of a macro-scale dry porous structure, i.e., \bar{K}_1 , \bar{E}_1 and M_1 , are numerically simulated by FEM. Instead of calculating the real elastic constants of the fluid-filled porous layers, here we only assume that the dry and fluid-filled porous layers have different effective Young's moduli, i.e., $\bar{E}_0=70\text{GPa}$ and $\tilde{E}_0=100\text{GPa}$, respectively. The Poisson's ratio of both layers is $\tilde{\nu}_0=\bar{\nu}_0=0.3$. Two cases with different macro-scale porosities, i.e., $\phi_1=0.4$ and $\phi_1=0.1$, are considered. The FEM models here are established in a similar manner to those in Section 3.1, including geometry and boundary conditions. More specifically, the model is a 2D porous plate with ordered pores, as illustrated in Fig. 1(c). Each unit cell in the model is composed of two layers, as shown in Fig. 6(c), in which the inner layer represents the fluid-filled skeleton and the outer layer represents the dry skeleton. By applying external loads, the effective moduli (i.e., \bar{E}_1 , \bar{K}_1 , and M_1) can be calculated directly. The normalized effective moduli with respect to Young's modulus \bar{E}_0 are plotted as a function of volume fraction of the fluid-filled skeleton layer in Fig. 7 with symbols. The corresponding theoretical predictions (Eqs. (3), (5) and (9) with $i=1$) are also included as solid lines for comparison. It is clearly shown that the theoretical predictions can consist with the FEM simulations well for both cases. With increasing the volume fraction of the fluid-filled layer, all moduli increase. This is because the modulus of the fluid-filled layer is larger than the dry layer and stiffens the composite structure.

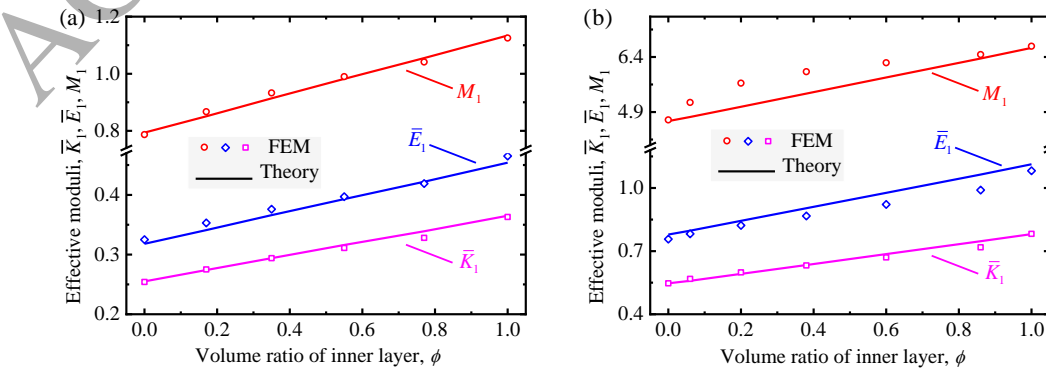


Fig. 7. Comparison of FEM simulations (symbols) and theoretical predictions (lines) of the effective elastic moduli of heterogeneous porous materials as a function of volume fraction of the fluid-filled porous layer: (a) $\phi_1 = 0.40$; (b) $\phi_1 = 0.10$.

4.2 Evolution of the effective properties during diffusion

When fluid is injected into the double-porosity structure, there are two typical stages. Firstly, the macro-scale pores are filled rapidly, incurring the stiffening of the structure. Secondly, pressurized fluid in the macro-scale pore diffuses into the micro-scale pores imbedded in the matrix, driven by the pressure gradient, resulting in complex changes of the overall elastic behavior. Relative to the second stage, the first one is much faster. Here we focus on the evolution of the effective properties during the fluid diffusion in the second stage.

Two typical injection conditions, i.e., constant pressure and constant injection rate, are considered. These conditions are common in practical engineering problems, such as CO₂ storage and hydraulic fracture (Coninck and Benson, 2014; Liu and Chen, 2015; Detournay, 2016). Following the filling of the macro-scale pores, the pressure can be held constant by controlling the fluid injection rate or alternatively, the injection rate can be held constant resulting in a change of pressure as fluid is redistributed during the diffusion process.

For the case of constant injection rate, learning from Boyer's Law for compressible fluids, a simple assumption can be employed to calculate the variable fluid pressure P_f as

$$P_f \cdot V_f = P_0 \cdot (V_0 + \dot{V} \cdot t) \quad , \quad (16)$$

where, following the initial filling of macro-pores, V_0 and P_0 are respectively the volume and pressure of injected fluids. The expression $V_f = V_0 \cdot \left\{ 1 + \left[(r/r_1)^2 - 1 \right] \cdot \phi_0 \right\}$ yields the volume of the redistributed fluid phase during the diffusion process. Here \dot{V} is the flow rate of injection during the diffusion process and can be defined by a

simple expression $\dot{V} = \kappa \cdot (V_0/t_0^*)$, with κ being a non-dimensional factor and t_0^* the initial value of the time scale t_0 (i.e., $t_0^* = t_0(P_0)$). Substituting the expressions of V_f and \dot{V} into Eq. (16), the variable fluid pressure P_f can be calculated as

$$P_0/P_f = 1 + \left[(r/r_1)^2 - 1 \right] \cdot \phi_0 - \kappa \cdot (t/t_0^*) , \quad (17)$$

which shows that the pressure P_f changes during the process of diffusion. For the special case of $\kappa=0$, no additional fluid is injected into the porous materials after the initial filling of the macropores. Thus, the situation reduces to the condition of constant fluid volume.

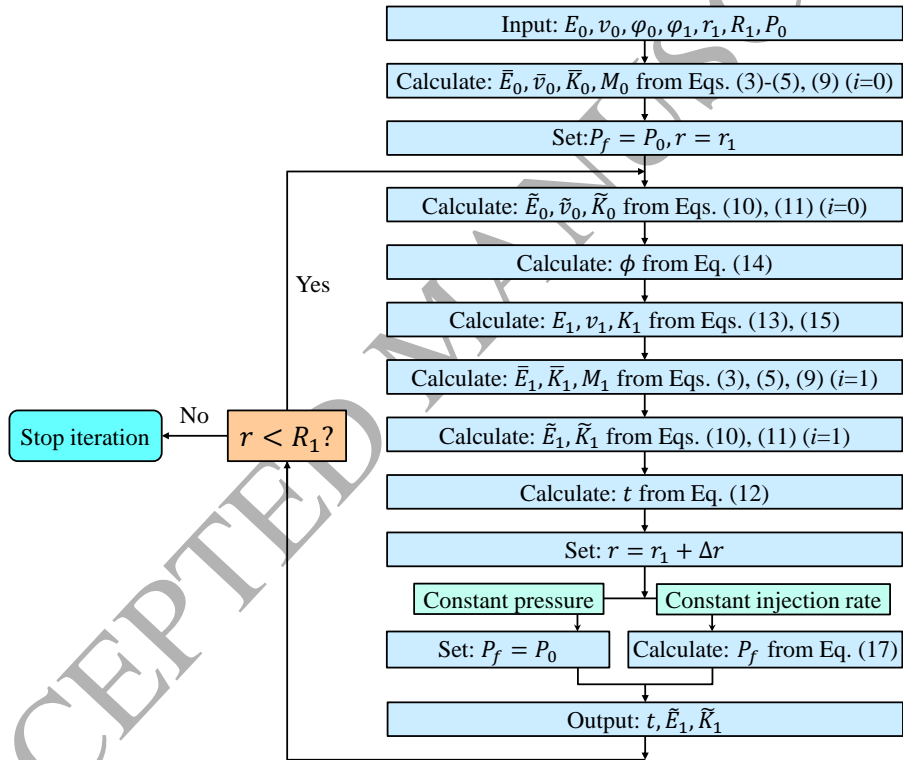


Fig. 8. Flow chart of the iterative algorithm used for determining the variation of effective properties of fluid-filled porous materials.

It should be noted that in evaluating pressure, the assumption inspiring from Boyer's law is only applicable for the highly compressible fluid but cannot be applied for cases of fluid with low compressibility. For the cases of the incompressible fluid, the diffusion process may be driven by other mechanisms, such as matrix suction. This compressibility simplification is imposed here to give a reasonable estimation of the

fluid pressure profile under the injection. Moreover, it is also worth noting that the capillary effect further plays a role at micropores when the fluid diffuses from the macropores into the non-continuum skeleton, and consequently the permeability of the skeleton will be changed during the diffusion process. Both the capillary effect and the permeability variation should be taken into account to further improve the accuracy of the present models.

It was shown in the previous section that as fluid diffuses from macro- into micro-scale pores, the effective properties of the non-continuum solid matrix are enhanced by the pressurized fluid. With the movement of the fluid front during the diffusion process, the thickness of the fluid-filled porous layer increases, whereas the thickness of the dry porous layer decreases. The overall elastic responses of the fluid-filled porous material change accordingly. The evolution of the effective properties can be captured through an iterative procedure, and the corresponding flow chart of the iterated algorithm is given in Fig. 8. The key point is that the pressure needs to be updated at each step for the constant injection rate condition.

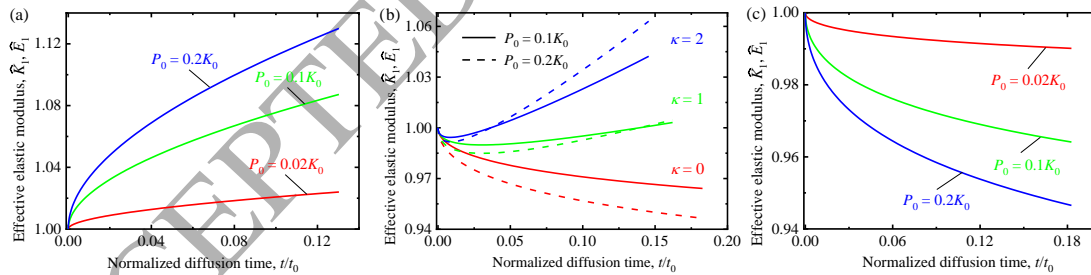


Fig. 9. Variation of normalized effective elastic moduli as functions of the normalized diffusion time under injection conditions of: (a) constant pressure; (b) constant injection rate and (c) constant volume.

Here we assume the constituent solid matrix of the micro-scale porous structure is linearly elastic with Young's modulus $E_0=70\text{GPa}$ and Poisson's ratio $\nu_0=0.3$. To simplify the analysis, both porosities at macro- and micro-scale are fixed at $\phi_0=\phi_1=0.5$. The theoretical predictions of the normalized effective elastic moduli are plotted as a function of the normalized diffusion time in Fig. 9. The effective moduli

are normalized by the corresponding initial value of each case before diffusion, i.e., $\tilde{E}_1(P_0)$ and $\tilde{K}_1(P_0)$. Therefore, the vertical coordinates in Fig. 9 indicate the relative variation of the effective moduli induced by fluid diffusion. Under the conditions of constant injection rate and constant volume, the time scale t_0 changes with varying P_f and the initial value t_0^* was used to normalize the diffusion time. Three initial pressures (i.e., $P_0 = 0.02K_0$, $0.1K_0$ and $0.2K_0$) are considered for both constant pressure and constant volume conditions. For the constant injection rate condition, two initial pressures ($P_0 = 0.1K_0$ and $0.2K_0$) with three sets of parameters, i.e., $\kappa = 0, 1$, and 2 , are considered. It is noted that the evolution rules for bulk modulus and Young's modulus are the same, due to the fact that the distribution of both moduli depends linearly on the local fluid pressure, as shown in Eqs. (10) and (11).

For the constant pressure conditions shown in Fig. 9(a), the effective moduli increase with increasing diffusion time for different initial pressures. This results in an increase in the fraction of pressurized micro-scale pores in the non-continuum solid matrix during the diffusion process. This effect stiffens the fluid-filled porous material. However, for conditions of constant injection rate, see Fig. 9(b), the evolution varies with injection rate and shows different tendencies over time. This behavior arises from two factors. On the one hand, the volume ratio of pressurized micro-scale pores increases during diffusion and strengthens the non-continuum solid matrix. On the other hand, due to the injection and redistribution of the fluid, the pressure will change in different ways under the different injection rates. These two factors, i.e., diffusion and injection, compete with each other and lead to the final evolutionary properties. As an extreme case of constant injection rate conditions, for constant volume conditions, decreasing effective moduli are found with increasing diffusion time for different initial pressures, as shown in Fig. 9(c). It also should be mentioned that the specific evolution law also depends on the porosities of both macro- and micro- porous structures. Here we presented the representative results for specific values of porosities at both scales as a numerical example. Further systematical

analyses with varied combinations of porosities at the two scales can be conducted following our proposed theoretical solutions presented here.

5 Discussion and conclusion

We have developed a multiscale framework for investigating the overall elastic response of fluid-filled porous materials with multiscale structures, on the basis of a micro-mechanical model with double-porosity. The effective properties of the dry porous material are predicted quantitatively based on a single-porosity model, and validated by FEM simulations. By introducing the geometric factor, the effect of pore distribution is taken into account. With these results, the effect of fluid pressure on the effective properties of porous materials is further investigated. The results show that the effective bulk modulus and Young's modulus are linearly dependent on fluid pressure. Additionally, according to the double-scale micromechanical model, the diffusion of fluid between macro- and micro-scale pores driven by the pressure gradient is considered. By applying an iterative algorithm, effective properties are predicted theoretically for injection conditions of constant pressure and constant injection rate.

The multiscale framework developed in this paper provides a tool to analyze the overall elastic response of fluid-filled porous materials and has implications towards the improvement of the design of sensors and actuators in various applications. As a typical example, estimating the storage performance of CO₂ injected into underground saline aquifers is an important problem in carbon geosequestration. It is also related to the safety assessment of the operation process. Saline aquifers are typical multiscale porous structures, and during the injection of CO₂, their overall mechanical properties will vary as CO₂ diffuses from macro- to micro-scale pores. By means of the theoretical model presented here, these effective properties can be correlated to the amount and distribution of CO₂. By applying acoustic detection technology (Van Den

Abeele et al., 2002), the effective properties of partially saturated saline aquifers can be measured, and then the stored amount of CO_2 therein can be accessed. However, here we only present a basic idea, and further in-depth studies are still needed for actual operations.

Additionally, it should be noted that the coupling between the pore pressure and solid skeleton in fluid-filled porous materials is, in general, bi-directional. In this work, to explore their pressure/diffusion-dependent effective properties, and at the same time to simplify the analysis, only unidirectional coupling, i.e., the effect of fluid pressure on solid deformation, is taken into account, and the reverse effect is neglected. In future studies, bi-directional coupling should be considered.

Furthermore, although this paper is limited to the elastic responses of porous materials with ordered 2D structures and excludes any random distribution of pores and the connectivity of the porous structures, the same methodology used in this paper can be extended to 3D porous structures with multiscale random pores. However, for the 3D porous structure, the effects of distribution and orientation of pores on the effective response requires further consideration.

Acknowledgments

This work is supported by the Science Challenge Project of China (Grant No. TZ2018007), and the National Natural Science Foundation of China (No. 11472149 and 11732007). M.L. acknowledges the support from the Endeavour Research Fellowship founded by Australian Government. Y.G. acknowledges the support from The University of Sydney SOAR Fellowship and the Australian Research Council Discovery Project DP170102886.

References

- Auriault, J.L., Boutin, C., 1992. Deformable porous media with double porosity. Quasi-statics. I: Coupling effects. *Transp. Porous Media* 7, 63–82.
- Auriault, J.L., Boutin, C., 1993. Deformable porous media with double porosity. Quasi-statics. II: Memory effects. *Transp. Porous Media* 10, 153–169.
- Ayyagari, R.S., Vural, M., 2016. On the nature of pressure dependence in foams. *Int. J. Solids Struct.* 78, 160–173.
- Ba, J., Nie, J.X., Cao, H., Yang, H.Z., 2008. Mesoscopic fluid flow simulation in double-porosity rocks. *Geophys. Res. Lett.* 35, L04303.
- Berryman, J.G., Wang, H.F., 1995. The elastic coefficients of double-porosity models for fluid transport in jointed rock. *J. Geophys. Res.* 100, 24611–24627.
- Biot, M.A., 1941. General theory of three-dimensional consolidation. *Journal of Applied Physics*, 12, 155–164.
- Borgomano, J.V.M., Pimienta, L., Fortin, J., Guéguen, Y., 2017. Dispersion and attenuation measurements of the elastic moduli of a dual-porosity limestone. *J. Geophys. Res.* 122, 2690–2711.
- Boutin C., Roye P., 2015. On models of double porosity poroelastic media. *Geophys. J. Int.* 203, 1694–1725.
- Brown, R. J., Korringa, J., 1975. On the dependence of the elastic properties of a porous rock on the compressibility of the pore fluid. *Geophys.* 40, 608–616.
- Brown, D. L., Popov, P., Efendiev, Y., 2014. Effective equations for fluid-structure interaction with applications to poroelasticity. *Appl. Anal.* 93, 771–790.
- Chen, F., Sevostianov, I., Giraud, A., Grgic, D., 2018. Combined effect of pores concavity and aspect ratio on the elastic properties of a porous material. *Int. J. Solids Struct.* 134, 161–172.
- Chen, Z., Wang, X., Giuliani, F., Atkinson, A., 2015. Microstructural characteristics and elastic modulus of porous solids. *Acta Mater.* 89, 268–277.
- Cheng A.H.D., 1997. Material coefficients of anisotropic poroelasticity. *Int. J. Rock Mech. Min. Sci.* 34, 199–205.
- Choo, J., White, J.A., Borja, R.I., 2016. Hydromechanical modeling of unsaturated flow in double porosity media. *Int. J. Geomech.* 16, D4016002.
- Christensen, N.I., Wang, H.F., 1985. The influence of pore pressure and confining pressure on dynamic elastic properties of Berea sandstone. *Geophys.* 50, 207–213.
- Christensen, R.M., 2012. *Mechanics of Composite Materials*. Courier Corporation.
- Coninck, H., Benson, S.M., 2014. Carbon dioxide capture and storage: issues and

prospects. *Annu. Rev. Env. Resour.* 39, 243–270.

Conrath, M., Fries, N., Zhang, M., Dreyer, M.E., 2010. Radial capillary transport from an infinite reservoir. *Transp. Porous Media* 84, 109–132.

Coussy, O., Dormieux, L., Detournay, E., 1998. From mixture theory to Biot's approach for porous media. *Int. J Solids Struct.*, 35, 4619–4635.

Cowin, S.C., 2001. *Bone Mechanics Handbook*, 2nd ed. CRC Press, Boca Raton, FL.

Day, A.R., Snyder, K.A., Garboczi, E.J., Thorpe, M.F., 1992. The elastic moduli of a sheet containing circular holes. *J. Mech. Phys. Solids* 40, 1031–1051.

Detournay, E., 2016. Mechanics of hydraulic fractures. *Annu. Rev. Fluid Mech.* 48, 311–339.

Dorodnitsyn, V., Van Damme, B., 2016. Two-dimensional fluid-filled closed-cell cellular solid as an acoustic metamaterial with negative index. *Phys. Rev. B* 93, 134302.

Georget, D.M.R., Smith, A.C., Waldron, K.W., 2003. Modelling of carrot tissue as a fluid-filled foam. *J. Mater. Sci.* 38, 1933–1938.

Gibson, L.J., Ashby, M.F., 1999. *Cellular Solids: Structure and Properties*. Cambridge University Press.

Gibson, L.J., Ashby, M.F., Harley, B.A., 2010. *Cellular Materials in Nature and Medicine*. Cambridge University Press.

Gor, G.Y., Bertinetti, L., Bernstein, N., Hofmann, T., Fratzl, P., Huber, P., 2015. Elastic response of mesoporous silicon to capillary pressures in the pores. *Appl. Phys. Lett.* 106, 261901.

Goussev, O.A., Richner, P., Rozman, M.G., Gusev, A.A., 2000. Void-containing materials with tailored Poisson's ratio. *J. Appl. Phys.* 88, 4013–4016.

Guiducci, L., Fratzl, P., Bréchet, Y.J., Dunlop, J.W., 2014. Pressurized honeycombs as soft-actuators: a theoretical study. *J. R. Soc. Interface* 11, 20140458.

Guo, F.L., He, B.B., Niu, X., 2015. Analysis of vapor pressure and void volume fraction evolution in porous polymers: a micromechanics approach. *Int. J. Solids Struct.* 66, 133–139.

Hu, N., Wang, B., Tan, G.W., Yao, Z.H., Yuan, W.F., 2000. Effective elastic properties of 2-D solids with circular holes: numerical simulations. *Comp. Sci. Tech.* 60, 1811–1823.

Kim, A.H., Guyer, R.A., (Eds.). 2014. *Nonlinear Elasticity and Hysteresis: Fluid-solid Coupling in Porous Media*. John Wiley & Sons.

Kitazono, K., Sato, E., Kuribayashi, K., 2003. Application of mean-field approximation to elastic-plastic behavior for closed-cell metal foams. *Acta Mater.* 51,

4823–4836.

Leung, D.Y., Caramanna, G., Maroto-Valer, M.M., 2014. An overview of current status of carbon dioxide capture and storage technologies. *Renew. Sustain. Energy Rev.* 39, 426–443.

Li, B., Wang, B., Reid, S.R., 2010. Effective elastic properties of randomly distributed void models for porous materials. *Int. J. Mech. Sci.* 52, 726–732.

Liu, M., Chen, C.Q., 2015. A micromechanical analysis of the fracture properties of saturated porous media. *Int. J. Solids Struct.* 63, 32–38.

Liu, M., Wu, J., Gan, Y., Chen, C.Q., 2016 (a). The pore-load modulus of ordered nanoporous materials with surface effects. *AIP Adv.* 6, 035324.

Liu, M., Wu, J., Gan, Y., Hanaor, D.A., Chen, C.Q., 2016 (b). Evaporation limited radial capillary penetration in porous media. *Langmuir* 32, 9899–9904.

Liu, M., Zhang, Y., Wu, J., Gan, Y., Chen, C.Q., 2016 (c). Analytical solutions for elastic response of coated mesoporous materials to pore pressure. *Int. J. Eng. Sci.* 107, 68–76.

Lv, J., Liu, H., Zhang, H.W., 2014. A multiscale co-rotational method for geometrically nonlinear shape morphing of 2D fluid actuated cellular structures. *Mech. Mater.* 79, 1–14.

Ma, L.H., Yang, Q.S., Yan, X.H., Qin, Q.H., 2014. Elastoplastic mechanics of porous materials with varied inner pressures. *Mech. Mater.* 73, 58–75.

Mackenzie, J.K., 1950. The elastic constants of a solid containing spherical holes. *Proc. Phys. Soc. B* 63, 2–11.

Moutsopoulos, K.N., Konstantinidis, A.A., Meladiotis, I.D., Tzimopoulos, C.D., Aifantis, E.C., 2001. Hydraulic behavior and contaminant transport in multiple porosity media. *Transp. Porous Media* 42, 265–292.

Pabst, W., Gregorová, E., Tichá, G., 2006. Elasticity of porous ceramics-A critical study of modulus – porosity relations. *J. Euro. Ceram. Soc.* 26, 1085–1097.

Rohan, E., Naili, S., Cimirman, R., Lemaire, T., 2012. Multiscale modeling of a fluid saturated medium with double porosity: Relevance to the compact bone. *J. Mech. Phys. Solids* 60, 857–881.

Rohan, E., Naili, S., Lemaire, T., 2016. Double porosity in fluid-saturated elastic media: deriving effective parameters by hierarchical homogenization of static problem. *Continuum Mech. Therm.* 28, 1263–1293.

Shafiro, B., Kachanov, M., 1997. Materials with fluid-filled pores of various shapes: Effective elastic properties and fluid pressure polarization. *Int. J. Solids Struct.* 34, 3517–3540.

Sobera, M.P., Kleijn, C. R., 2006. Hydraulic permeability of ordered and disordered

single-layer arrays of cylinders. *Physical Review E* 74, 036301.

Song, Y., Hu, H., Rudnicki, J.W., 2016. Shear properties of heterogeneous fluid-filled porous media with spherical inclusions. *Int. J. Solids Struct.* 83, 154–168.

Spadoni, A., Höhler, R., Cohen-Addad, S., Dorodnitsyn, V., 2014. Closed-cell crystalline foams: self-assembling, resonant metamaterials. *J. Acoust. Soc. Am.* 135, 1692–1699.

Streit, J.E., Hillis, R.R., 2004. Estimating fault stability and sustainable fluid pressures for underground storage of CO₂ in porous rock. *Energy* 29, 1445–1456.

Su, B., Zhou, Z., Xiao, G., Wang, Z., Shu, X., Li, Z., 2017. A pressure-dependent phenomenological constitutive model for transversely isotropic foams. *Int. J. Mech. Sci.* 120, 237–248.

Szulczewski, M.L., MacMinn, C.W., Juanes, R., 2014. Theoretical analysis of how pressure buildup and CO₂ migration can both constrain storage capacity in deep saline aquifers. *Int. J. Greenhouse Gas Control*, 23, 113–118.

Thompson, M., Willis, J.R., 1991. A reformation of the equations of anisotropic poroelasticity. *J Appl. Mech.*, 58, 612–616.

Timoshenko, S., Goodier, J., 1970. *Theory of Elasticity*, 3rd ed. McGraw-Hill book Company.

Tsakiroglou, C.D., Ioannidis, M.A., Amiritharaj, E., Vizika, O., 2009. A new approach for the characterization of the pore structure of dual porosity rocks. *Chem. Eng. Sci.* 64, 847–859.

Van Den Abeele, K. A., Carmeliet, J., Johnson, P. A., Zinszner, B., 2002. Influence of water saturation on the nonlinear elastic mesoscopic response in Earth materials and the implications to the mechanism of nonlinearity. *J. Geophys. Res.* 107, 2121.

Vincent, P.G., Monerie, Y., Suquet, P., 2009. Porous materials with two populations of voids under internal pressure: I. Instantaneous constitutive relations. *Int. J. Solids Struct.* 46, 480–506.

Walsh, J.B., Brace, W.F., England, A.W., 1965. Effect of porosity on compressibility of glass. *J. Am. Ceram. Soc.* 48, 605–608.

Wang, J.C., 1984. Young's modulus of porous materials. *J. Mater. Sci.* 19, 801–808.

Wang, G., Tu, W., Pindera, M. J., 2017. Tailoring the moduli of composites using hollow reinforcement. *Comp. Struct.* 160, 838–853.

Warner, M., Thiel, B.L., Donald, A.M., 2000. The elasticity and failure of fluid-filled cellular solids: theory and experiment. *Proc. Nat. Acad. Sci.* 97, 1370–1375.

Whitaker, S., 1986. Flow in porous media I: A theoretical derivation of Darcy's law. *Transp. Porous Media* 1, 3–25.

Yuk, H., Lin, S., Ma, C., Takaffoli, M., Fang, N.X., Zhao, X., 2017. Hydraulic hydrogel actuators and robots optically and sonically camouflaged in water. *Nat. Commun.* 8, 14230.

ACCEPTED MANUSCRIPT